Rapid Communications

Nonmonotonic diffusion rates in an atom-optics Lévy kicked rotor

Sanku Paul,[1] Sumit Sarkar,[2] Chetan Vishwakarma,[2] Jay Mangaonkar,[2] M. S. Santhanam,[2] and Umakant Rapol[2]
[1]*Max-Planck-Institut für Physik Komplexer Systeme, Nöthnitzer Straße 38, 01187-Dresden, Germany*
[2]*Indian Institute of Science Education and Research, Homi Bhabha Road, Pune 411 008, India*

(Received 8 July 2019; published 4 December 2019)

The dynamics of chaotic Hamiltonian systems such as the kicked rotor continues to guide our understanding of transport and localization processes. The localized states of the quantum kicked rotor decay due to decoherence effects if subjected to noise. The associated quantum diffusion increases monotonically as a function of a parameter characterizing the noise distribution. In this Rapid Communication, for the atom-optics Lévy kicked rotor, the quantum diffusion displays nonmonotonic behavior as a function of a parameter characterizing the Lévy distribution. The optimal diffusion rates are experimentally obtained using an ultracold cloud of rubidium atoms in a pulsed optical lattice. The parameters for optimal diffusion rates are obtained analytically and show a good agreement with our experimental and numerical results. The nonmonotonicity is shown to be a quantum effect that vanishes in the classical limit.

DOI: 10.1103/PhysRevE.100.060201

Chaotic Hamiltonian systems continue to open up novel scenarios for momentum and energy transport in both the classical and quantum regimes. The kicked rotor system, a particle periodically kicked by an external sinusoidal field, is a paradigm for Hamiltonian chaos [1]. This sets a standard benchmark for momentum transport, namely that, in the regime of sufficiently strong kicking strengths, the onset of quantum interference effects suppresses the classical diffusive transport [2,3]. This is the dynamical localization scenario in which the system settles into a quasisteady state without absorbing further energy. In contrast to this, novel transport scenarios have been exemplified by several variants of a kicked rotor. These include atom-optics-based experimental realizations and theoretical studies of directed transport in parity-broken [4], $\mathcal{PT}$-symmetric [5], and dissipative [6] kicked rotors. Anomalous transport has been observed in Lévy kicked [7], relativistic [8,9], and a nonsmooth version [10] of a kicked rotor, while suppression of quantum diffusion was observed in higher-dimensional [11], nonideal [12], coupled [13,14], and relativistic [15] kicked rotors. As the quantum kicked rotor is related to the Anderson model [16,17] for charge transport in a crystalline lattice, all of these results have applications in a larger class of disordered conductors and time-dependent problems in condensed matter physics.

The kicked rotor system is suitable for studying decoherence and/or the quantum to classical transition of its localized states, especially since the classical and quantum signatures of transport are markedly distinct. In the classical domain, the temporal evolution of mean energy is $\langle E\rangle = Dt$ where the diffusion coefficient $D \approx K^2/2$ and K is the kick strength [2]. In the corresponding quantum regime, $\langle E\rangle$ becomes asymptotically time independent, i.e., $\langle E\rangle = Dt^*[1-\exp(-t/t^*)]$, where t^* is the localization timescale until which quantum dynamics follows the classical behavior. Thus, the numerical values of the kick strength $K \gg 1$ and kick period T determine the classical and quantum diffusion rates [2]. In particular, varying K does not alter the qualitative nature of diffusion except if the accelerator modes are present in the classical phase space [18,19]. On the other hand, if the parameters K and/or T are subjected to stationary noise, i.e., K is replaced by $K+\delta K$, where δK is drawn from a stationary probability distribution, then both theory and experiments have shown that quantum localization is not sustained [20–22]. A similar scenario unfolds if T is subjected to an additive noise [23]. In general, increasing the tunable noise strength leads to quantum diffusion that monotonically approaches the classical limit. In many situations where conductivity, and not localization, is desired, the tunability for optimal transport with a fixed kicked strength is useful.

In this Rapid Communication, we propose and demonstrate a mechanism based on manipulating the periodic kick sequence by tuning a parameter associated with Lévy-noise characteristics to obtain optimal momentum transport in an atom-optics kicked rotor (AOKR) system. Experimentally, the existence of the optimal diffusion rate as a function of a parameter characterizing the noise distribution is demonstrated. The observed results are in good agreement with the analytical results and simulations.

We consider the dimensionless Hamiltonian of the quantum AOKR given by

$$H = \frac{p^2}{2} + K\cos(x)\sum_n (1-g_n)\delta(t-n). \tag{1}$$

In this, g_n is a stochastic variable that controls whether an external field of kick strength K is applied to the cold atomic cloud at the nth time instant. Further, g_n is taken from a discrete Bernoulli distribution such that if $g_n = 0$, the particle experiences a kick, and if $g_n = 1$, no kick is applied. The waiting time between the occurrences of 0 is drawn from a Lévy waiting time distribution $w(\tau) \sim \tau^{-1-\alpha}$, where α is the Lévy exponent [24,25]. The regime of $0 < \alpha < 1$ corresponds to a diverging mean waiting time $\bar{\tau}$ and, as we had demonstrated earlier, this effectively leads to a slower decay of decoherence

[7]. In this Rapid Communication, we exploit the dynamics when the kicks are imparted at time intervals governed by $w(\tau)$ with exponent $\alpha > 1$ and $\bar{\tau} = \frac{\alpha}{\alpha-1}$ is well defined. In this regime, we demonstrate through both theory and experimentation the existence of an optimal quantum diffusion as a function of α. This optimality is an unusual property since for other commonly used additive noise sources such as white and Gaussian noise, quantum diffusion is usually monotonic as a function of noise strength [25,26]. Early experimental attempts at manipulating the kick sequence without introducing noise, such as the double kicked rotors, modify the standard diffusion due to kick-to-kick correlations or classical cantori [27] but do not lead to nonmonotonicity and optimality in diffusion rates.

The quantum dynamics of the system in Eq. (1) for $\alpha > 1$ is studied using a Floquet analysis. The Floquet operator can be written as

$$F(K_n) = e^{-ip^2/2\hbar_s}\, e^{-iK\cos x/\hbar_s}\, e^{-iK'_n \cos x/\hbar_s} = F(K)F(K'_n), \tag{2}$$

where $\hbar_s$ is the scaled Planck's constant, $K_n = K(1 - g_n)$, and $K'_n = -Kg_n$. Further, $F(K)$ represents the Floquet operator of the standard kicked rotor $F(K) = e^{-ip^2/2\hbar_s}\, e^{-iK\cos x/\hbar_s}$ for which $g_n = 0$ for all n. The noisy rotor corresponds to $F(K'_n)$. We consider the eigenstate $|r\rangle$ of the Floquet operator $F(K)$ given by

$$F(K)|r\rangle = e^{-i\eta_r}|r\rangle,$$

where η_r is the quasienergy of the state $|r\rangle$. For $K \gg 1$ as we have taken, $|r\rangle$ would be localized states. The factor g_n induces noise in the kicking sequence whenever $g_n = 1$, i.e., the time instances when the kicks are not imparted. Thus, under the action of $F(K'_n)$, the system transitions from state $|r\rangle$. The survival probability amplitude $A_r(t', t'')$ of the noisy system to remain in the state $|r\rangle$ in a given time interval $[t'', t')$ [25] is

$$A_r(t', t'') = \mathcal{N}\langle r|\mathcal{T}\prod_{n=t''}^{t'-1} F(K_n)|r\rangle, \tag{3}$$

in which $\mathcal{T}$ represents time ordering and $\mathcal{N} = e^{-i\eta_r(t'-t'')}$ is introduced to normalize the survival probability amplitude for the noiseless system.

By using random-phase approximations and averaging over all the quasienergy states and also over the random phases of the initial state, the survival probability amplitude is

$$A_r(t', t'') = q(K'_n/\hbar_s)^{G(t',t'')}. \tag{4}$$

In this, $G(t', t'')$ represents the number of noisy events in the interval $[t'', t')$ and

$$q(K'_n/\hbar_s) = 1 - \left(K'^2_n/2!\,\hbar_s^2\right)\overline{\cos^2(x)} + \left(K'^4_n/4!\,\hbar_s^4\right)\overline{\cos^4(x)} + \cdots. \tag{5}$$

Since $|q(K'_n/\hbar_s)| < 1$ for $K'_n \neq 0$, the survival probability in the state $|r\rangle$ decays over time and the consequent state transitions result in diffusion. By using the force-force correlator which is related to the decoherence factor [25,28,29], the mean energy for $\alpha > 1$ can be obtained as

$$\langle E\rangle_t \sim \frac{K^2}{2}(1 - e^{\frac{-t}{t^*}}) - \frac{K^2}{2\alpha}t + \frac{K^2}{2}\frac{t}{1-\frac{\alpha}{c}} + O(q^t) \sim I_1 + I_2 + I_3 + O(q^t), \tag{6}$$

where $c = (q^2 - 1)t^*$ and $t^* \sim \frac{K_n^2}{\hbar_s^2}$ is the localization time (or break time) of the standard kicked rotor. To physically understand this expression, we analyze each of these terms. The first term $I_1 = \frac{K^2}{2}(1 - e^{\frac{-t}{t^*}})$ represents the energy growth of the standard kicked rotor, $I_2 = -\frac{K^2}{2\alpha}t$ corresponds to the missing of kicks, and the energy growth represented by $I_3 = \frac{K^2}{2}\frac{t}{1-\frac{\alpha}{c}}$ results from decoherence due to the introduction of noise.

After long times, $t \gg t^*$, Eq. (6) reduces to $\langle E\rangle \sim Dt$, in which the diffusion coefficient D is given by

$$D \sim \frac{K^2}{2}\left(-\frac{1}{\alpha} + \frac{1}{1-\frac{\alpha}{c}}\right). \tag{7}$$

This reveals a nonlinear dependence of the diffusion coefficient D on both the kick strength K and Lévy exponent α. The mean energy of the system grows linearly in time, indicating a dominance of diffusion. In contrast, the diffusion coefficient D has a quadratic dependence on kick strength but the dependence on α is not monotonic. The expressions in Eqs. (6) and (7) form the central analytical results of this Rapid Communication. In what follows, we describe an atom-optics-based experiment to verify these results.

The experimental setup and the sequence is similar to that in Refs. [7,30]. We prepare a laser-cooled cloud of ^{87}Rb atoms in the magneto-optical trap (MOT). This is followed by further forced evaporative cooling in a crossed optical dipole trap ($\lambda = 1064$ nm). The cold atomic ensemble has $\sim 2 \times 10^5$ atoms at temperature $\sim 3\ \mu$K and follows the Maxwell-Boltzmann distribution in momentum space. This atomic ensemble serves as the initial Gaussian wave packet for simulating the quantum kicked rotor. The process of kicking is implemented using a pulsating one-dimensional (1D) optical lattice. The lattice laser beam is $\sim$6.7 GHz detuned to the red from the $|F = 1\rangle \longrightarrow |F' = 2\rangle$ transition of ^{87}Rb. The lattice beam is derived from the first-order diffraction of an acousto-optic modulator (AOM). The lattice is turned on and off by switching the rf power that drives the AOM via a high-frequency switch. The pulse on time for the applied kicks is ≈ 220 ns and the free propagation time is kept to be $\approx$10.6 μs. For the parameters used in the experiment, the scaled Planck constant is $\sim$2 and the kick strength K is calculated to be 6 with a 10% uncertainty. For realization of the Lévy noise, a sequence of waiting times following Lévy statistics is fed into an arbitrary wave-form generator which in turn controls the rf switch of the AOM driver. The presented experimental data for each Lévy exponent are an average over five different noise realizations.

Figure 1(a) shows one realization of the actual kicking sequence used in the experiment for several values of the Lévy exponent α. As α increases, the mean number of missed kicks

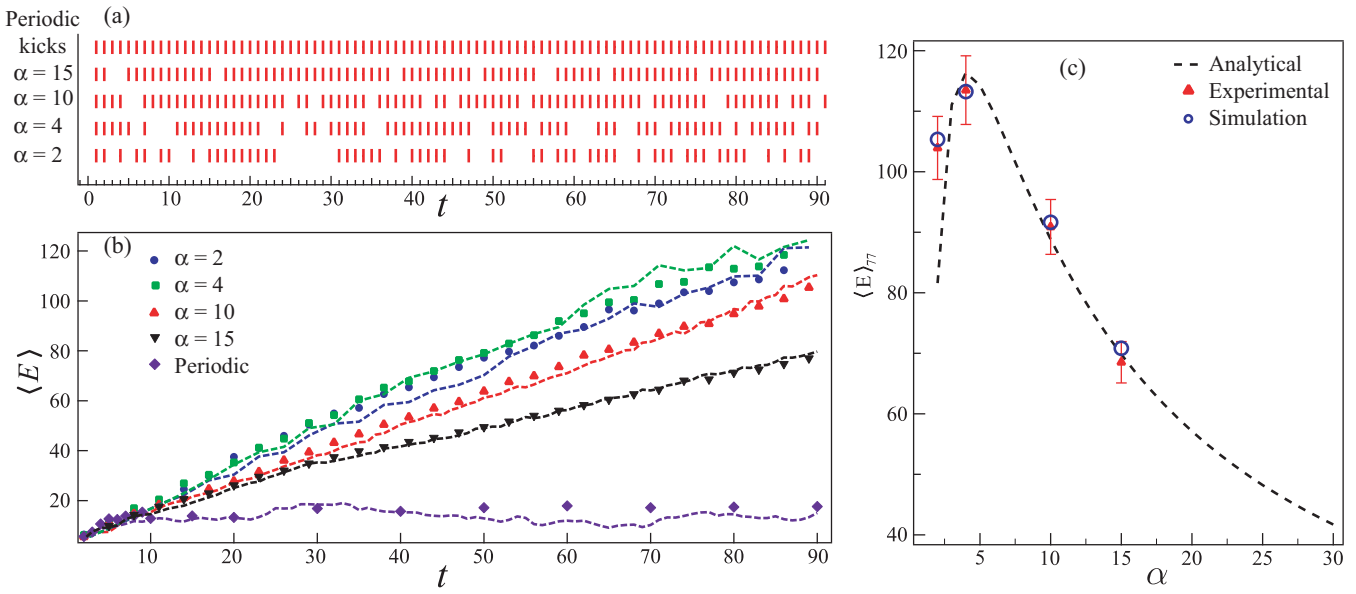

FIG. 1. (a) Schematic diagram of the sequence of kicks that are experimentally applied by pulsing the rf driving an acousto-optic modulator that switches the optical lattice on/off. (b) Measured (symbols) and numerically simulated (dashed lines) mean energy growth for $\alpha = 2, 4, 10,$ and 15 with $K = 6.0$, $\hbar_s = 2.0$. Experimental values have $\pm 5\%$ uncertainty (not shown in the figure). (c) Quantum diffusion coefficient as a function of α. Mean energy after 77 kicks is plotted as a function of α for $K = 6.0$, $\hbar_s = 2.0$. Triangles represent experimental measurements, open circles are the numerically computed values, and the dashed line is the analytical expression in Eq. (7).

decreases such that, in the limit of $\alpha \to \infty$, it is effectively a periodic kick sequence. In this limit, we expect the system to display the properties of a standard kicked rotor system, i.e., Eq. (1) with $g_n = 0$ for all n. Figure 1(b) shows the mean energy growth of the system for $K = 6$, $\hbar_s = 2$ while the Lévy exponent α is varied. In this figure, symbols represent experimental measurements while dashed lines are the numerical results.

To obtain a broader perspective of this result, for an arbitrarily chosen time $t = \bar{t}$, the mean energy $\langle E \rangle_{\bar{t}}$ is tracked as a function of α. Figure 1(c) shows the case of $\bar{t} = 77$ (in units of kick period) with $K = 6.0$, $\hbar_s = 2.0$, for experimental measurements matched against numerical simulations and the analytical expression in Eq. (7). For the latter, the localization time t^* is treated as a fitting parameter and found to be $t^* = 5.84$. Clearly, the experimental result displays an excellent agreement with the theoretical result in Eq. (7). Notably, there is a finite α, $\alpha = \alpha_c$, at which $\langle E \rangle_{\bar{t}}$ (and therefore D) is maximum. In the case shown in Fig. 1(c), $\alpha_c \approx 4.0$. The choice of $t = 77$ is for illustrative purposes. A similar behavior with an identical value of α_c is obtained for any other t, provided other parameters are held constant. Physically, the nonmonotonic behavior of the diffusion coefficient results from the competition between the two terms, I_2 (energy loss from missing of kicks) and I_3 (the overall increase in mean energy due to decoherence of the localized state). As shown below, this is purely a quantum effect absent in the corresponding classical system.

Further, we explore the limit of $\alpha \to \infty$. For any fixed value of t such that $t \gg t^*$, if the limit $\alpha \gg \alpha_c$ is taken, both I_2 and I_3 tend to zero. This leads to $\langle E \rangle \sim K^2/2$, a time-independent value corresponding to that of the localized state obtained with periodic kicking. For large α, the mean number of missed kicks becomes vanishingly small and hence the system essentially works as a standard kicked rotor. As observed in Fig. 1(c), for large α, the mean energy approaches a constant value. This constant value of $K^2/2 = 18$ is approached very slowly since $D \propto \alpha^{-1}$ as $\alpha \to \infty$. This can be expected for $\alpha \gg 1$ for any finite value of $\hbar_s$. However, for moderately large α in the semiclassical limit of $\hbar_s \to 0$, consistent with the discussion in Ref. [31], the diffusion timescale dominates over the noise timescale, and hence quantum diffusion approximately follows the classical.

In Figs. 2(a) and 2(b), numerically simulated energy diffusion of the system in Eq. (1) is displayed for $K = 10$ and 15, respectively. It can be noticed from comparing the two figure panels that α_c depends on the kick strength. For $K = 10$,

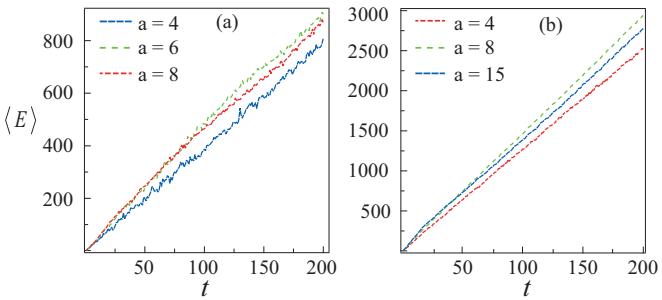

FIG. 2. Numerically calculated mean energy growth of the system as a function of time t with (a) kick strength $K = 10$, $\hbar_s = 2$ (top curve is for $\alpha = 6$, middle curve is for $\alpha = 8$, and the bottom curve for $\alpha = 4$) and (b) $K = 15$, $\hbar_s = 2$ (top curve is for $\alpha = 8$, middle curve is for $\alpha = 15$, and the bottom curve is for $\alpha = 4$).

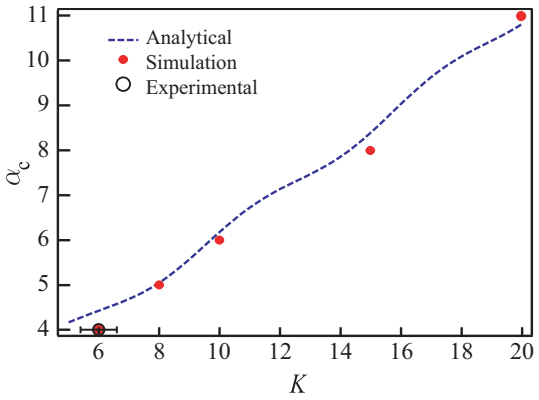

FIG. 3. The variation of critical exponent α_c as a function of K, with $\hbar_s = 2$. The dashed line is the analytical expression in Eq. (8) and symbols represent the values of α_c from numerical simulations. At $K = 6$, experimental data for α_c from Fig. 1(c) are also shown.

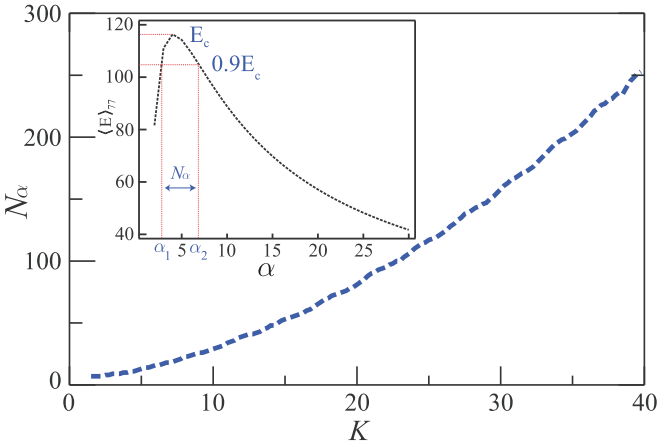

FIG. 4. Simulations showing the variation of $N_\alpha (= \alpha_2 - \alpha_1)$ with K. The values of α_1 and α_2 are chosen such that $\langle E \rangle$ is 90% of that at α_c. The inset shows the analytical result from Fig. 1(c). In this, E_c is the mean energy at α_c and N_α is the "bandwidth" in α.

$\alpha_c \approx 6$, and for $K = 15$, we obtain $\alpha_c \approx 8$. These numerical estimates of α_c agree with those predicted by the analytical expression in Eq. (8). The results shown in Figs. 1(b) and 1(c) are qualitatively similar for other values of kick strengths as well, while maintaining the dependence of maximum α_c on K. For a fixed value of time $t = \bar{t}$, starting from Eq. (7) an expression for α_c is derived by extremizing D with respect to α and it gives

$$\alpha_c = \frac{1 + \sqrt{(1-q^2)t^*}}{1 - \frac{1}{(1-q^2)t^*}}. \tag{8}$$

In this, $q \equiv q(K_n'/\hbar_s)$ and $t^* \equiv t^*(K/\hbar_s)$. Hence, α_c depends only on the ratio $\frac{K}{\hbar_s}$. Figure 3 shows α_c as a function of K for a fixed value of $\hbar_s$. In this figure, the result of Eq. (8) is matched against the numerical simulations of a quantum Lévy kicked rotor. The experimentally obtained data point for $K = 6$ is also shown. To a first approximation, α_c increases linearly with K. This result also emphasizes the quantum nature of the nonmonotonic diffusion in a Lévy kicked rotor. As $\hbar_s \to 0$, in the semiclassical limit, $K/\hbar_s \gg 1$ and hence $\alpha_c \to \infty$. Hence, the nonmonotonic diffusion is a quantum phenomenon and cannot be seen in the classical Lévy kicked rotor. Indeed, in the classical numerical simulations (not shown here) of this system, the diffusion is indeed monotonic for all values of K.

Another feature that can be inferred from Fig. 2 is that for large kick strengths such as $K \gtrapprox 10$, the curves for $\langle E \rangle_t$ corresponding to different values of α tend to be close to each other or even overlap. However, for $K = 6$ in Fig. 1, as α is varied, $\langle E \rangle_t$ remains quite distinct. The extent to which the system responds to variations in the Lévy exponent α can be quantified by a "response" curve defined as follows. We define a "bandwidth" in α space (see the inset in Fig. 4) as $N_\alpha = \alpha_2 - \alpha_1$, in which α_1 and α_2 are such that

$$\langle E \rangle_t(\alpha_1) = \langle E \rangle_t(\alpha_2) = 0.9 \langle E \rangle_t(\alpha_c), \quad \text{and} \quad \alpha_2 > \alpha_1. \tag{9}$$

Thus, in analogy with the Q values of the oscillators, smaller values of N_α would correspond to a higher sensitivity of the system to changes in α, in stark contrast to larger N_α corresponding to lower sensitivity. Figure 4 shows N_α obtained through numerical simulations starting from Eq. (6). The inset in this figure pictorially illustrates the definition of N_α for the data shown in Fig. 1(c). It is seen that as K increases, N_α increases, pointing to increasing loss of sensitivity to changes in α for large kick strengths. This behavior of N_α explains why $\langle E \rangle_t$ curves nearly overlap for large K. If $K \gg 1$, there is a wide band of α values for which diffusion rates are nearly the same as those at α_c. Physically, it is reasonable to expect that large kick strengths are classically chaotic regimes, and the AOKR is less sensitive to variations in α.

In summary, the dynamics of a Lévy kicked rotor system is studied through experiments, theory, and simulations. In this variant of a kicked rotor, the system misses kicks at time intervals governed by the Lévy waiting time distribution, $w(\tau) \sim \tau^{-1-\alpha}$, with $\alpha > 1$. The central result is nonmonotonic behavior of the diffusion coefficient upon variation of α. Physically, nonmonotonicity of diffusion arises due to the competition between noise-induced energy loss (arising from missing kicks) and the energy gain due to decoherence effects. In general, for any value of kick strength K such that the system is classically chaotic, the diffusion rate as a function of α displays a single maximum at $\alpha = \alpha_c$. The theoretical result shows that $\alpha_c \propto K/\hbar_s$, implying that the nonmonotonic diffusion is a purely quantum effect that vanishes in the classical limit.

U.R. and C.V. would like to thank the Council of Scientific and Industrial Research (CSIR), New Delhi, India for funding. We acknowledge Jamie McLennan for a critical reading of the manuscript.

S.P. and S.S. contributed equally to this work. S.P. performed the theoretical and computational work. S.S. was part of the experimental team.

[1] B. V. Chirikov, Phys. Rep. **52**, 263 (1979); B. B. Chirikov, F. M. Izrailev, and D. L. Shepelyansky, Sov. Sci. Rev., Sect. C **2**, 209 (1981).
[2] H. J. Stöckmann, *Quantum Chaos: An Introduction* (Cambridge University Press, Cambridge, U.K., 2000).
[3] F. Haake, *Quantum Signatures of Chaos* (Springer, Berlin, 2013).
[4] C. Hainaut, A. Rancon, J. F. Clement, J. C. Garreau, P. Szriftgiser, R. Chicireanu, and D. Delande, Phys. Rev. A **97**, 061601(R) (2018).
[5] S. Longhi, Phys. Rev. A **95**, 012125 (2017).
[6] G. G. Carlo, L. Ermann, A. M. F. Rivas, and M. E. Spina, Phys. Rev. E **93**, 042133 (2016).
[7] S. Sarkar, S. Paul, C. Vishwakarma, S. Kumar, G. Verma, M. Sainath, U. D. Rapol, and M. S. Santhanam, Phys. Rev. Lett. **118**, 174101 (2017).
[8] D. U. Matrasulov, G. M. Milibaeva, U. R. Salomov, and B. Sundaram, Phys. Rev. E **72**, 016213 (2005).
[9] Q. Zhao, C. A. Muller, and J. Gong, Phys. Rev. E **90**, 022921 (2014).
[10] S. Paul, H. Pal, and M. S. Santhanam, Phys. Rev. E **93**, 060203(R) (2016); S. Paul and M. S. Santhanam, *ibid.* **97**, 032217 (2018).
[11] I. Manai, J. F. Clement, R. Chicireanu, C. Hainaut, J. C. Garreau, P. Szriftgiser, and D. Delande, Phys. Rev. Lett. **115**, 240603 (2015).
[12] F. Revuelta, R. Chacón, and F. Borondo, Phys. Rev. E **98**, 062202 (2018).
[13] S. Notarnicola, F. Iemini, D. Rossini, R. Fazio, A. Silva, and A. Russomanno, Phys. Rev. E **97**, 022202 (2018).
[14] P. Qin, A. Andreanov, H. C. Park, and S. Flach, Sci. Rep. **7**, 41139 (2017).
[15] L. Huang, H.-Y. Xu, C. Grebogi, and Y.-C. Lai, Phys. Rep. **753**, 1 (2018); E. B. Rozenbaum and V. Galitski, Phys. Rev. B **95**, 064303 (2017).
[16] D. R. Grempel, R. E. Prange, and S. Fishman, Phys. Rev. A **29**, 1639 (1984).
[17] P. W. Anderson, Phys. Rev. **109**, 1492 (1958); *50 Years of Anderson Localization*, edited by E. Abrahams (World Scientific, Singapore, 2010).
[18] A. Iomin, S. Fishman, and G. M. Zaslavsky, Phys. Rev. E **65**, 036215 (2002).
[19] M. B. d'Arcy, R. M. Godun, D. Cassettari, and G. S. Summy, Phys. Rev. A **67**, 023605 (2003).
[20] B. G. Klappauf, W. H. Oskay, D. A. Steck, and M. G. Raizen, Phys. Rev. Lett. **81**, 1203 (1998)
[21] D. A. Steck, V. Milner, W. H. Oskay, and M. G. Raizen, Phys. Rev. E **62**, 3461 (2000).
[22] H. Ammann, R. Gray, I. Shvarchuck, and N. Christensen, Phys. Rev. Lett. **80**, 4111 (1998).
[23] W. H. Oskay, D. A. Steck, and M. G. Raizen, Chaos, Solitons & Fractals **16**, 409 (2003).
[24] G. M. Zaslavsky, Phys. Rep. **371**, 461 (2002).
[25] H. Schomerus and E. Lutz, Phys. Rev. A **77**, 062113 (2008).
[26] H. Schomerus and E. Lutz, Phys. Rev. Lett. **98**, 260401 (2007).
[27] C. E. Creffield, G. Hur, and T. S. Monteiro, Phys. Rev. Lett. **96**, 024103 (2006); P. H. Jones, M. M. Stocklin, G. Hur, and T. S. Monteiro, *ibid.* **93**, 223002 (2004); K. Vant, G. Ball, H. Ammann, and N. Christensen, Phys. Rev. E **59**, 2846 (1999).
[28] D. Cohen, Phys. Rev. Lett. **67**, 1945 (1991); Phys. Rev. A **44**, 2292 (1991).
[29] J. Schriefl, M. Clusel, D. Carpentier, and P. Degiovanni, Europhys. Lett. **69**, 156 (2005).
[30] Details of the experiment are given in Supplemental Material of Ref. [7].
[31] E. Ott, T. M. Antonsen, Jr., and J. D. Hanson, Phys. Rev. Lett. **53**, 2187 (1984).